Supplementary information, Data S1

Materials and Methods

Clinical samples

   Insulinomas were diagnosed by clinical hypoglycemia symptoms, blood insulin and glucose levels (prolonged oral glucose tolerance test), computed tomography/positron emission tomography computed tomography imaging of patients and pathological diagnosis of surgical removal tumor, Cushing's disease and ACTH-secreting pituitary adenomas subtypes, pheochromocytoma and paraganglioma, aldosterone-producing adenomas were diagnosed according to clinical features, drug history, hormones tests, CT/MRI imaging and pathological diagnosis of surgical removal tumor. Genomic DNA was obtained from matched frozen tumor and blood samples in the endocrine-related tumor bank of Shanghai Key Laboratory for Endocrine Tumors. DNA was prepared with QIAGEN DNeasy Blood & Tissue Kit. Informed consent was obtained from all study participants. All the protocols were approved by the Rui-Jin Hospital Ethics Committee, Shanghai Jiao Tong University School of Medicine.

Whole-exome sequencing (WES) and targeted deep sequencing (TDS)

   The qualified genomic DNA from tumor and matched peripheral blood from tumors were fragmented by Covaris technology, and then adapters were ligated to both ends of the fragments. Extracted DNA was then amplified by ligation-mediated PCR, purified and hybridized to human exome array for enrichment, non-hybridized fragments were then washed out. Whole exome sequencing were performed for Insulinomas with NimbleGenEZ 44M kit, as pheochromocytomas, paraganglioma and pituitary adenomas with Agilent SureSelect Human All Exon v4 (51 Mb) kit. Target deep sequencing were performed for aldosterone-producing adenomas with NET panel of NimbleGen SeqCap EZ Designs.

Each captured library was then loaded on Hiseq2000 platform, and we performed high-throughput sequencing for each captured library independently to ensure that each sample meet the desired average fold-coverage. Raw image files were processed by Illumina base calling Software 1.7 for base calling with default parameters and the sequences of each individual were generated as 90 bp paired-end reads.

INSs, CDs and APAs were pooled and sequenced in Beijing Genomics Institute at Shenzhen, as PCC/PGLs in CapitalBio Corporation (Beijing, China).

Reads Mapping and Variation Detection

After removing reads containing sequencing adapters and low-quality reads with more than five unknown bases, high-quality reads were aligned to the NCBI human reference genome (hg19) using Burrows-Wheeler Aligner (v0.5.9)[11] with default parameters. Picard (v1.54)[12] was employed to mark duplicates and followed by Genome Analysis Toolkit (v1.0.6076, GATK IndelRealigner)[13] to improve alignment accuracy.

Somatic SNVs were detected by VarScan2.2.5[14] based on BWA align algorithm and high confident somatic SNVs were called if the following criteria were met: (I) both the tumor and normal samples should be covered sufficiently ($\geq 10\times$) at the genomic position; (II) the variants should be supported by at least 10% (5% for pituitary adenomas due to low purity) of the total reads in the tumor while less than 2% in the normal; (III) the variants should be supported by at least three reads in the tumor; (IV) distance between adjacent somatic SNVs distance should be over 10 bp; (V) mapping qualities of reads supporting mutant allele in tumor should be significantly higher than 30 (Wilcoxon rank sum test, $P < 0.2$); (VI) base qualities of reads supporting mutant allele in tumor should be significantly higher than 20 (Wilcoxon rank sum test, $P < 0.05$); (VII) mutations should not be enriched within 5 bp 5' or

3' of read end (Wilcoxon rank sum test, $P < 0.1$); (VIII) mutant allele frequency changes between tumor and blood should be statistically significant (Fisher's exact test, $P < 0.05$).

High confident somatic insertions and deletions (InDels) were called using the following steps: (I) candidate somatic InDels were predicted with GATK SomaticIndel Detector with default parameters; (II) for each predicted somatic indel, local realignment was performed with combined normal and tumor bam files; (III) frequent of variant reads less than 10% were filtered out. (IV) high confident somatic InDels were defined after filtering germline events.

Standardization and tracking of mutation data from 21 neuroendocrine tumors

In total, we collected mutations of 21 types of from 38 NGS projects[10, 15-40]. To make our data analysis more reliable, we established our data collection criteria as follows: (1) Metastasis samples were removed; (2) Tumor samples from same patients were removed; (3) Familial samples were removed.

Finally, all mutations were re-annotated by in-house annotation software based on snpeff[41-44]. To remove common sequencing artefacts or residual germline variation, each mutation was subjected to dbSNP database[45], and a 'Panel of Normal' filtering process using a panel of over 600 BAM files from 600 whole-exome sequencing or whole-genome sequencing normal samples at BGI-Shenzhen. Mutations observed in dbSNP or more than 1% in the panel of normal were removed.

Candidate driver genes analysis

We divided 512 samples from 14 types of benign tumor as combined benign set and 591 samples from 8 types of malignant tumors as combined malignant set in this project, because of the significant difference of mutation background between them. Candidate driver

genes of 21 NETs were identified in combined benign set, combined malignant set, combined organ set (adrenal, gastrointestinal, pituitary and thyroid) and individual tumor types.

Candidate driver genes were defined after two steps. In the first step, we selected genes that were significantly mutated than the background using MuSiC[46] package (FDR <= 0.2, Likelihood Ratio Test) in combined benign set, combined malignant set and individual tumor types. Furthermore, we performed an independent significant analysis that was restricted to events in genes that presented in Cancer Gene Census[47]. In the second step, genes met conditions as follows were filtered: (1) Mutation number less than 1% in sets; (2) Deleterious mutation rate less than 50%, deleterious mutations included mutations that were predicted to be deleterious by either SIFT[48] or PolyPhen-2[49], mutations in splicing region, and InDels in coding regions as well; (3) Genes that were low expressed or typically expressed in individual human tissue (log2 (RMA) > 5, from BioGPS[50]). Additionally, we manually added known driver genes from literature.

GO enrichment analysis

Significant molecular function GO term of 86 candidate driver genes were enriched using DAVID (https://david.ncifcrf.gov/).

Tumor specificity analysis

We calculate standard *Z*-score to make quantitative inferences as to the number of tumor types with which an individual gene or cellular process associates. The frequency of gene or cellular process was converted to a *Z*-score based on the descriptive statistics (mean and standard deviation) of the distribution in tumors.

Mutation VAF analysis

We computed the VAFs of somatic mutations in 86 candidate driver genes. Only mutation sites having > 100× coverage and candidate driver genes having at least 3 mutations were included in downstream analyses.

Protein-protein interaction networks

Functional interpretation for protein-protein interaction network of SMGs is generated by InWeb IM[51] (https://omictools.com/inweb-inbiomap-tool).

Therapeutic targets analysis

We grouped therapeutic agents within the categories in FDA approved, agents in cancer clinical trials, and agents in cancer pre-clinical ligands from target databases, literature, the drug's FDA label (www.fda.gov), or ClinicalTrials.gov (http://clinicaltrials.gov/). Gene and therapeutic agents' interactions were mainly retrieved from the TARGET database[52], Cancer bioMarkers database (www.cancergenomeinterpreter.org/biomarkers) and Gene Drug Knowledge Database[53].

To find new direct targeting interactions missed by these databases, we retrieved information of protein-molecule direct interactions from ChEMBL[54] (v20), a manually curated chemical database of bioactive molecules. We considered strong interactions, with a binding affinity more potent than 1 μM (pActivity > 6) described before[55]. We collected the following types of therapeutic agent: (1) FDA approved drug: interaction between an FDA approved drug and its targets, extracted by ChEMBL database and FDA label. (2) Drug in clinical trials: interactions between driver proteins and clinical trials molecules, with a binding affinity more potent than 1 μM (pActivity > 6), extracted by ClinicalTrials.gov. (3) Pre-clinical ligands: interactions between a pre-clinical molecule and a protein with a binding affinity higher that 1 μM (pActivity > 6). Here we included all interacting molecules either recorded in www.fda.gov as FDA approved or found in ClinicalTrials.gov.

To find druggable mutations, we used a script to connect mutations in NETs to drug responses using evidence from the [www.cancergenomeinterpreter.org/biomarkers], which is available for research use under a Creative Commons dedication. Mutations in druggable gene identified from ChEMBL were manually checked according to literature, www.fda.gov or ClinicalTrials.gov.

Clinically relevant events analysis

We computationally sort a patient's somatic variants with applying rules that rank variants based on the clinical and biological relevance as the methods described previously[56], which uses the TARGET database, MSigDB[57], COSMIC and CGC. We added drugable genes in NETs to these databases and then sorted somatic variants in each sample in NETs. Level of targets were defined as follows: A, clinically actionable mutations of NETs, actionable mutations were usually defined as known mutational hotspots, missense mutations in protein kinase regions with directionality known to have clinical impact, such as *RET* M918T; B, mutations in actionable cancer genes of NETs including therapeutic targets genes defined as earlier in the methods and genes with directionality known to have clinical impact; C, COSMIC mutations in CGC genes; D, mutations in genes that affected drugable linked pathway; E, mutations in genes that affected cancer related pathway; F, mutations in COSMIC; G, unknown mutations.
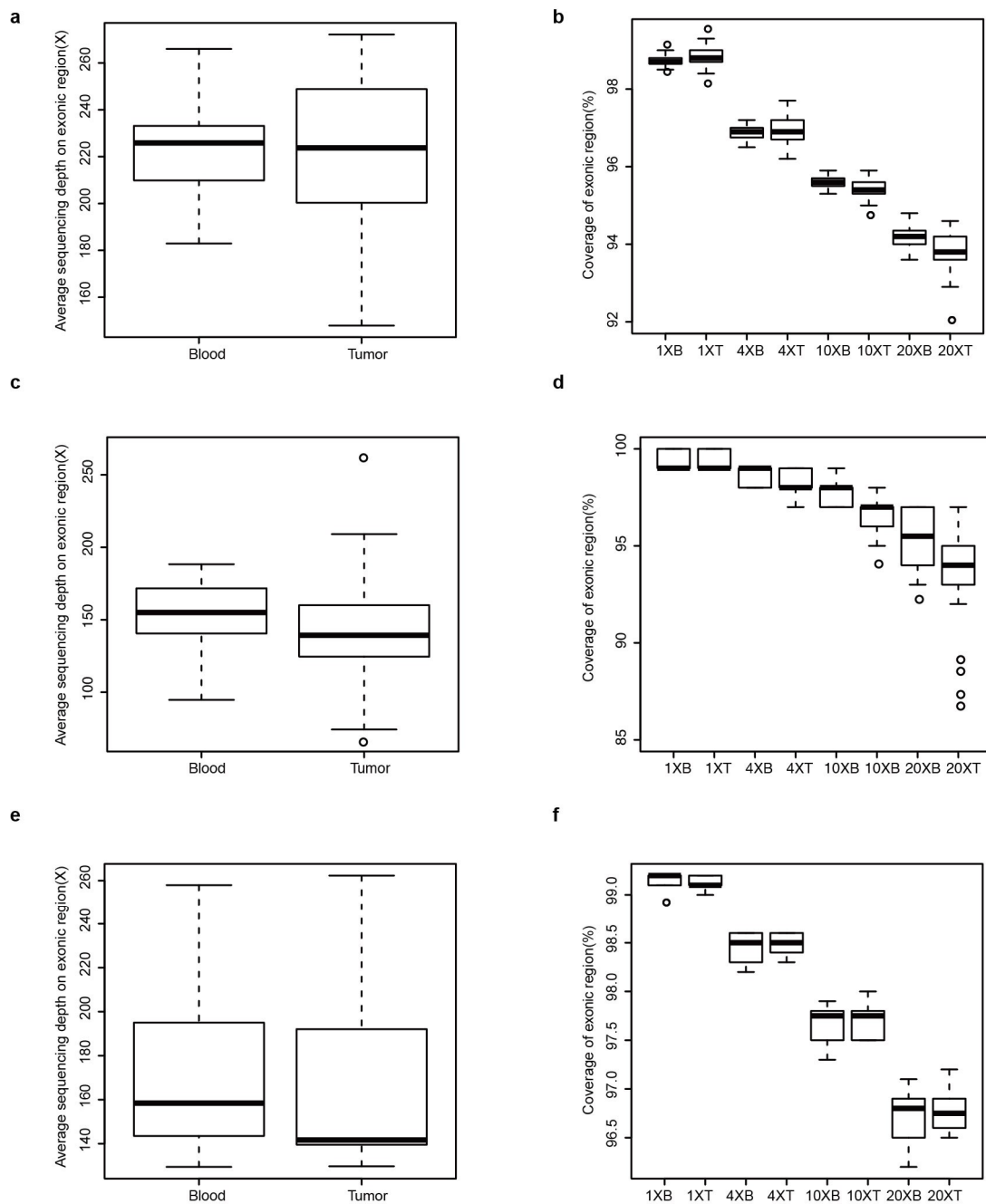
Supplementary information, Figure S1

a

b

c

d

e

f

Figure S1 Fold coverage of exonic regions for the pairs of CD, INS and PCC/PGL tumors. The average sequencing depth was 172×, and 96.8% (93.5%-98.5%) of the target regions were covered at least 10×. **(a)** The box plots show the distribution of average sequencing depth of exonic regions obtained from 40 pituitary Cushing's disease samples whole-exome sequencing data. The bold lines in boxes represent the medians and the lines outside the boxes represent the first or third quartiles of fold coverage.

(b) The box plots show the fraction of target bases covered by at least 1 reads, 4 reads, 10 reads and 20 reads across the 40 pituitary Cushing's disease samples. The bold lines in boxes show the medians and the lines outside the boxes show the first or third quartiles of fraction of target bases covered by reads. **(c)** The box plots show the distribution of average sequencing depth of exonic regions obtained from 76 insulinomas samples whole-exome sequencing data. The bold lines in boxes represent the medians and the lines outside the boxes represent the first or third quartiles of fold coverage. **(d)** The box plots show the fraction of target bases covered by at least 1 reads, 4 reads, 10 reads and 20 reads across the 76 insulinomas samples. The bold lines in boxes show the medians and the lines outside the boxes show the first or third quartiles of fraction of target bases covered by reads. **(e)** The box plots show the distribution of average sequencing depth of exonic regions obtained from 22 pheochromocytomas samples whole-exome sequencing data. The bold lines in boxes represent the medians and the lines outside the boxes represent the first or third quartiles of fold coverage. **(f)** The box plots show the fraction of target bases covered by at least 1 reads, 4 reads, 10 reads and 20 reads across the 22 pheochromocytomas. The bold lines in boxes show the medians and the lines outside the boxes show the first or third quartiles of fraction of target bases covered by reads.

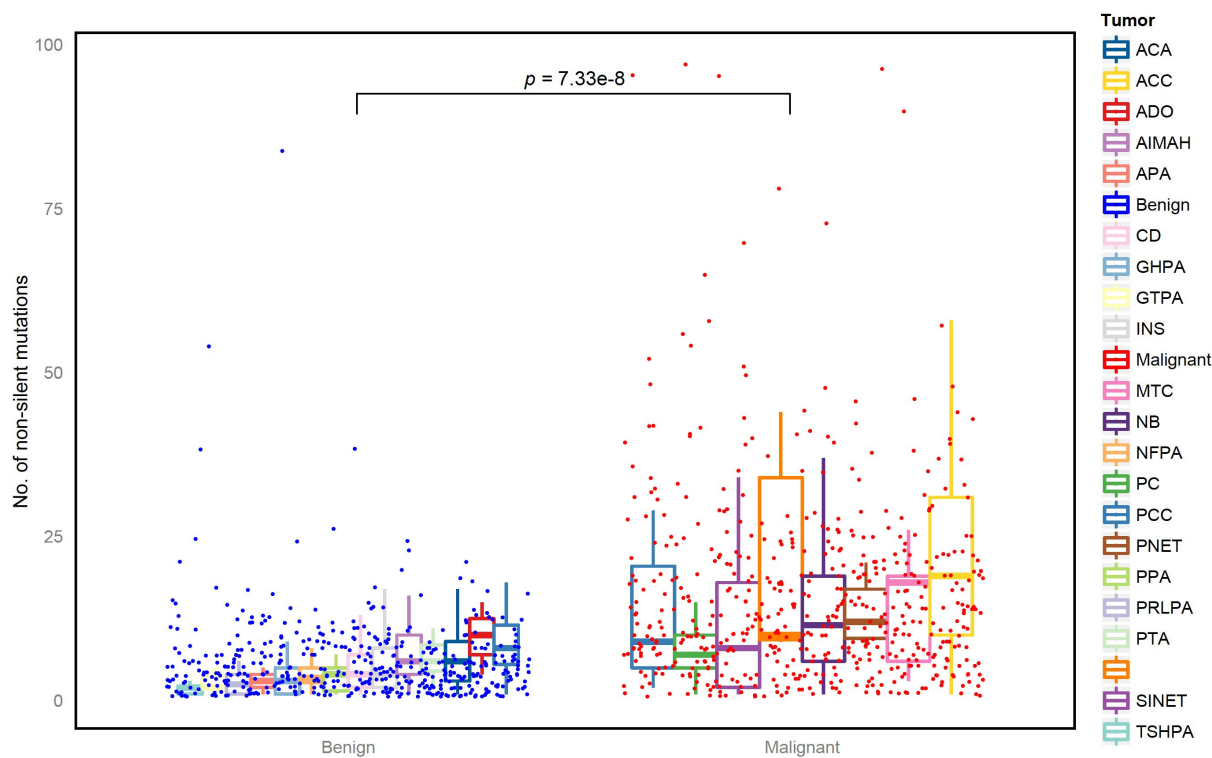# Supplementary information, Figure S2

Figure S2 Mutation frequencies between benign and malignant tumors. The NETs mutation dataset included a total of 16905 somatic mutations, consisting of 14039 missense, 1150 nonsense, 20 non-stop, 43 start lost, 478 splice-site and 1175 indels, including 960 frameshift and 215 inframeshift. The number of mutations per tumor varied between 1 and 1528. Student's *t*-test (one-sided) was applied to test significant difference.
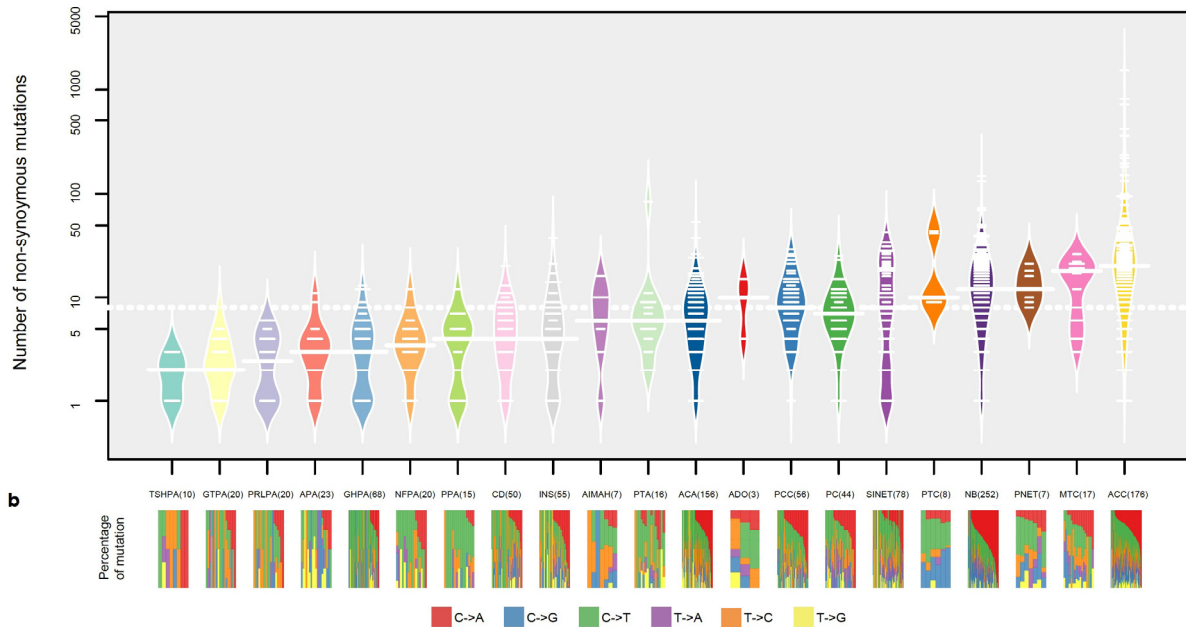
a

b

Figure S3 Mutation rate and spectrum across 21 NET types. (a) Distribution of mutation frequencies across 21 NETs. Tumors are clustered and presented with short lines in each tumor type, the length of the short lines in a bean plot indicates the number of times that tumors contain mutations. Solid white lines refer to the median for each NET type and dashed grey refers to the average across 21 NETs. TSHPA and GHPA has the lowest (median: 2; range 1-3), whereas ACC has the highest (median: 20; range 1-1528) median mutation frequency. PC has the lowest (median: 7; range 1-25) mutation frequency in malignant NETs, which is consistent with the nature of low-grade malignant tumors with benign behaviors[6]. **(b)** Mutation spectrum of transversion and transition categories for each NET type. C->T transversion is the predominant substitution in most tumor types.

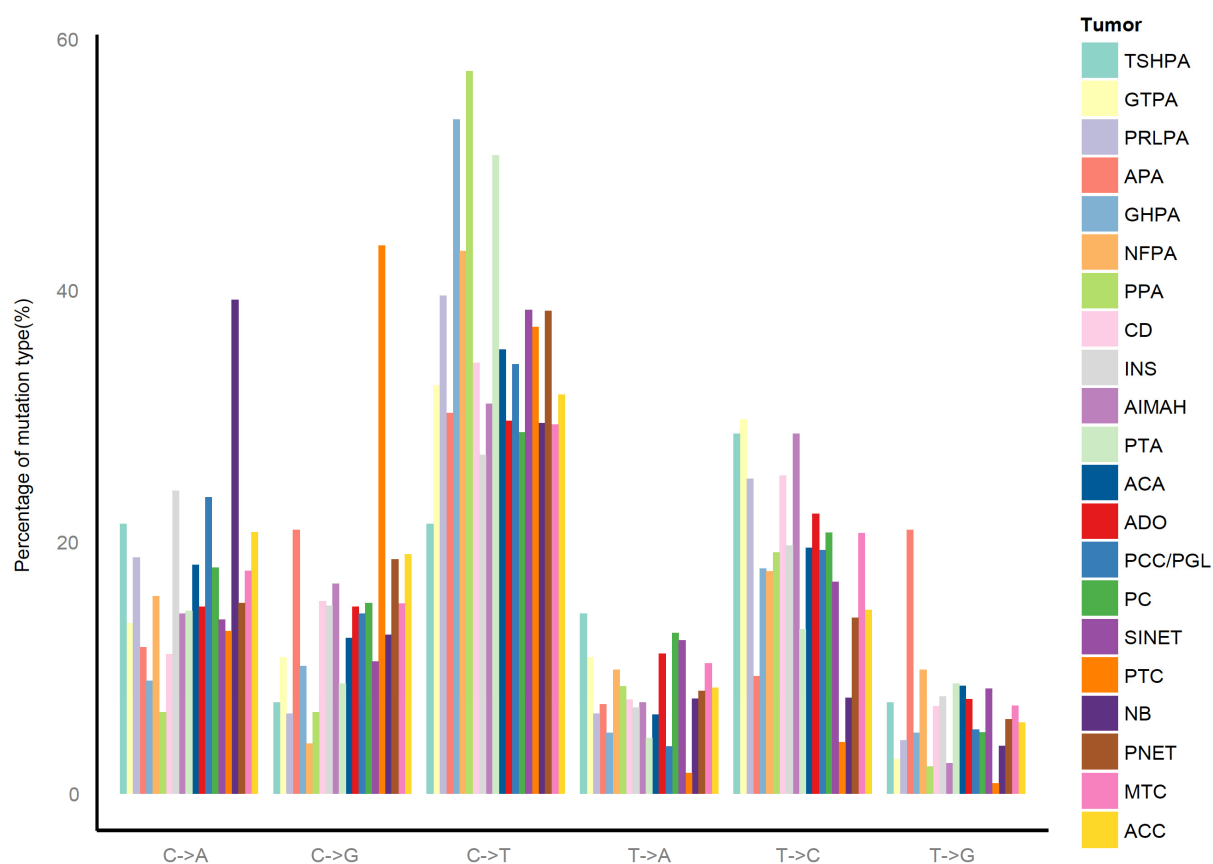# Supplementary information, Figure S4

Figure S4 Mutation spectrum in 21 neuroendocrine tumors. Spectrum of non-silent SNVs observed in exon regions in 21 neuroendocrine tumors. Tumors with hypermutations were excluded.
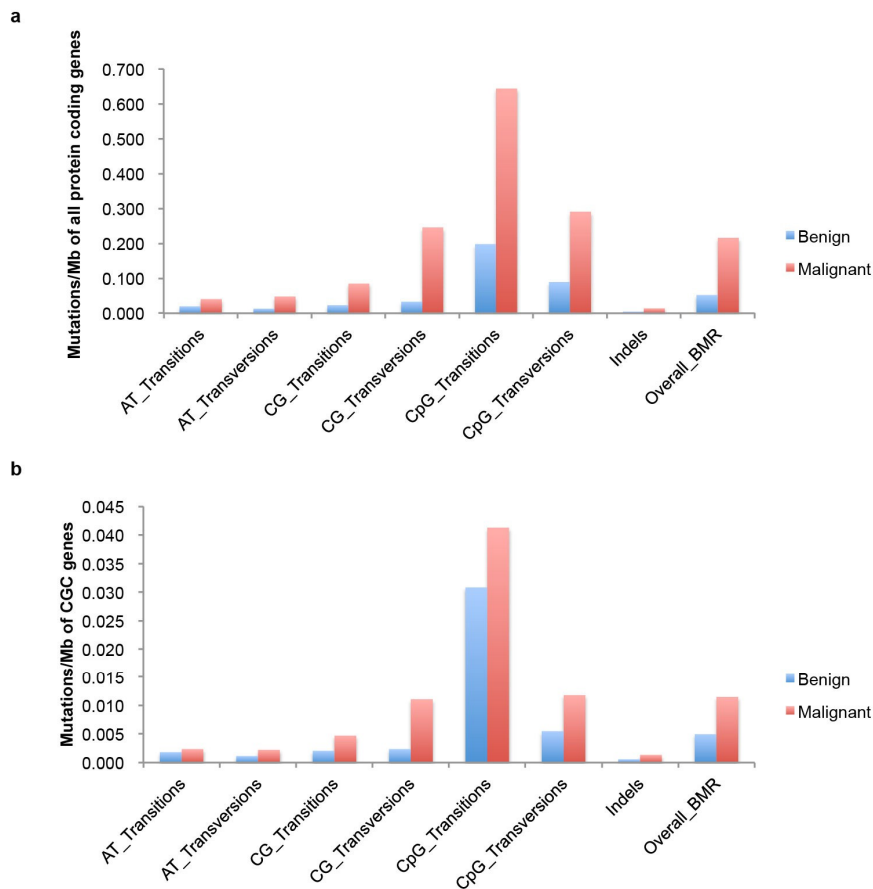
Supplementary information, Figure S5

Figure S5 Background mutation rates for benign and malignant tumors. (a) The background mutation rates (BMR) of non-silent mutations in whole exonic genes are plotted. Seven mutational mechanism categories are defined by MuSiC. The overall BMR is also plotted, combining all types of mutations. The BMR between benign and malignant tumors is different with $P = 0.029$ (*t*-test, one-sided). **(b)** The BMR of all non-silent mutations in genes from Cancer Gene Census for all seven mutational mechanism categories are plotted. The BMR between benign and malignant tumors is different with $P = 0.058$ (*t*-test, one-sided).

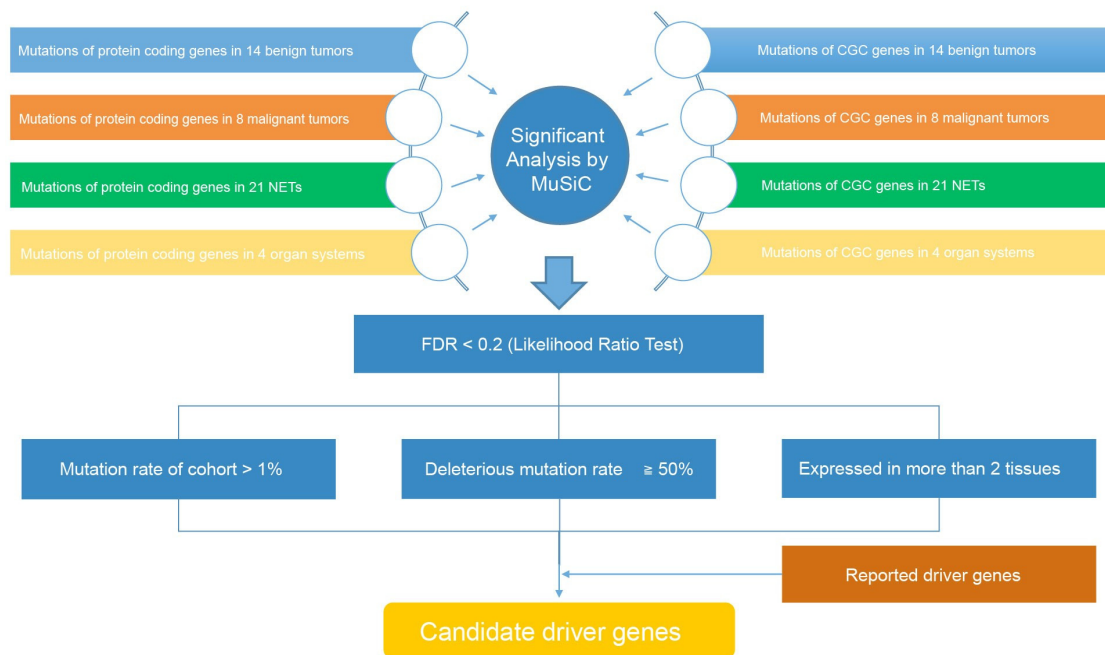# Supplementary information, Figure S6

Figure S6 Method of candidate driver gene analysis. We divided 512 samples from 14 types of benign tumor as combined benign set and 591 samples from 8 types of malignant tumors as combined malignant set. Candidate driver genes were identified in combined benign set, combined malignant set, combined organ set (adrenal, gastrointestinal, pituitary and thyroid) and individual tumors.

Supplementary information, Figure S7

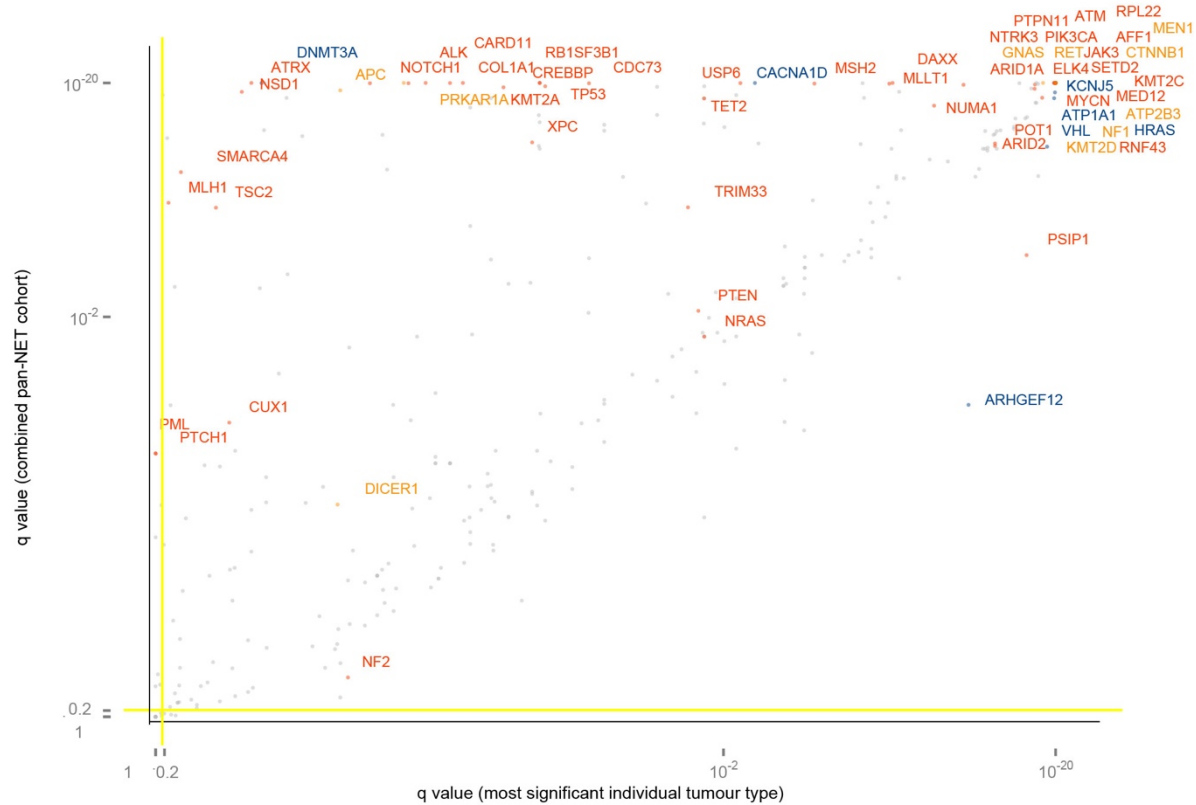**a**
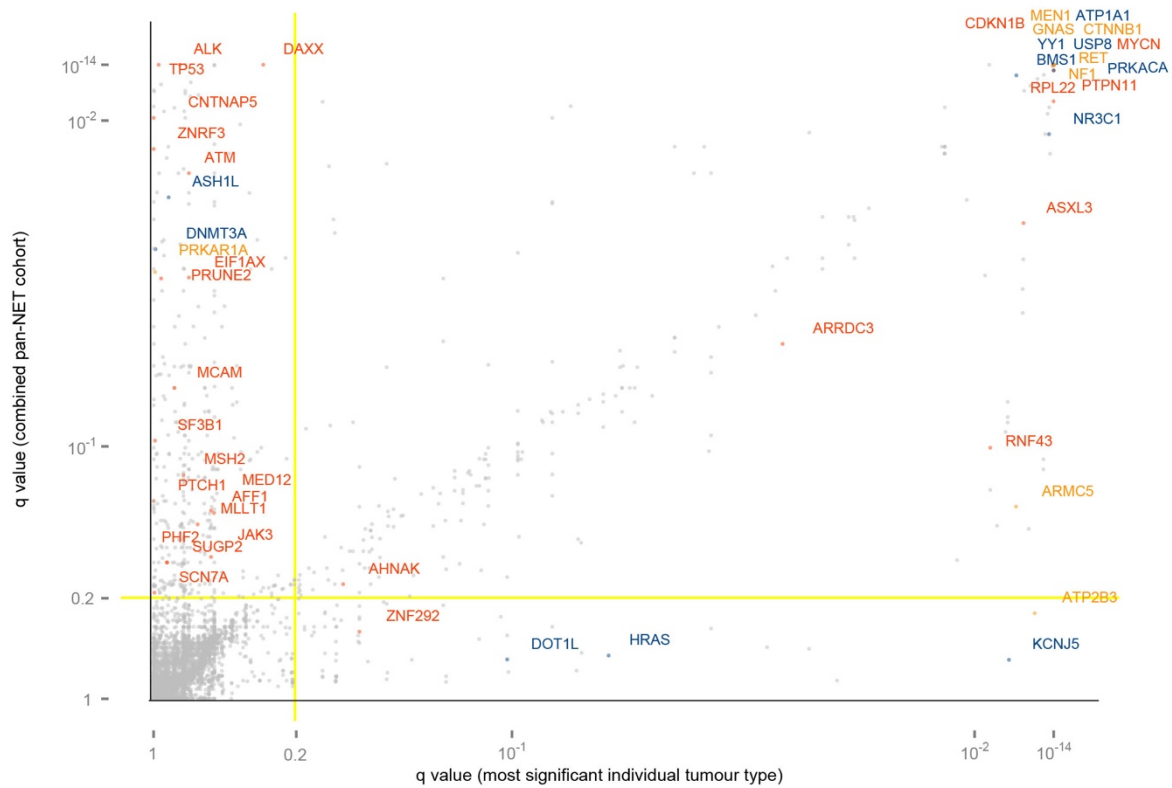
b

Figure S7 The significance of 86 candidate driver genes identified from 21 NETs. (a) All candidate driver genes are plotted by the *q* value (FDR) in the most significant of the individual 21 NETs (x axis) and the *q* value more significant among the combined benign tumors, combined malignant tumors and 4 organ cohorts (y axis). Color of gene names is as follows: red, only significant in malignant tumors; blue, only significant in benign tumors; orange, significant in both malignant and benign tumors. **(b)** Genes of Cancer Gene Census are plotted by the *q* value (FDR) in the most significant of the 21 NETs (x axis) and the *q* value more significant between the combined tumors, combined malignant tumors and 4 organ sets (y axis). The gene colors are marked as follows: red, only significant in malignant tumors; blue, only significant in benign tumors; orange, significant in both malignant and benign tumors.
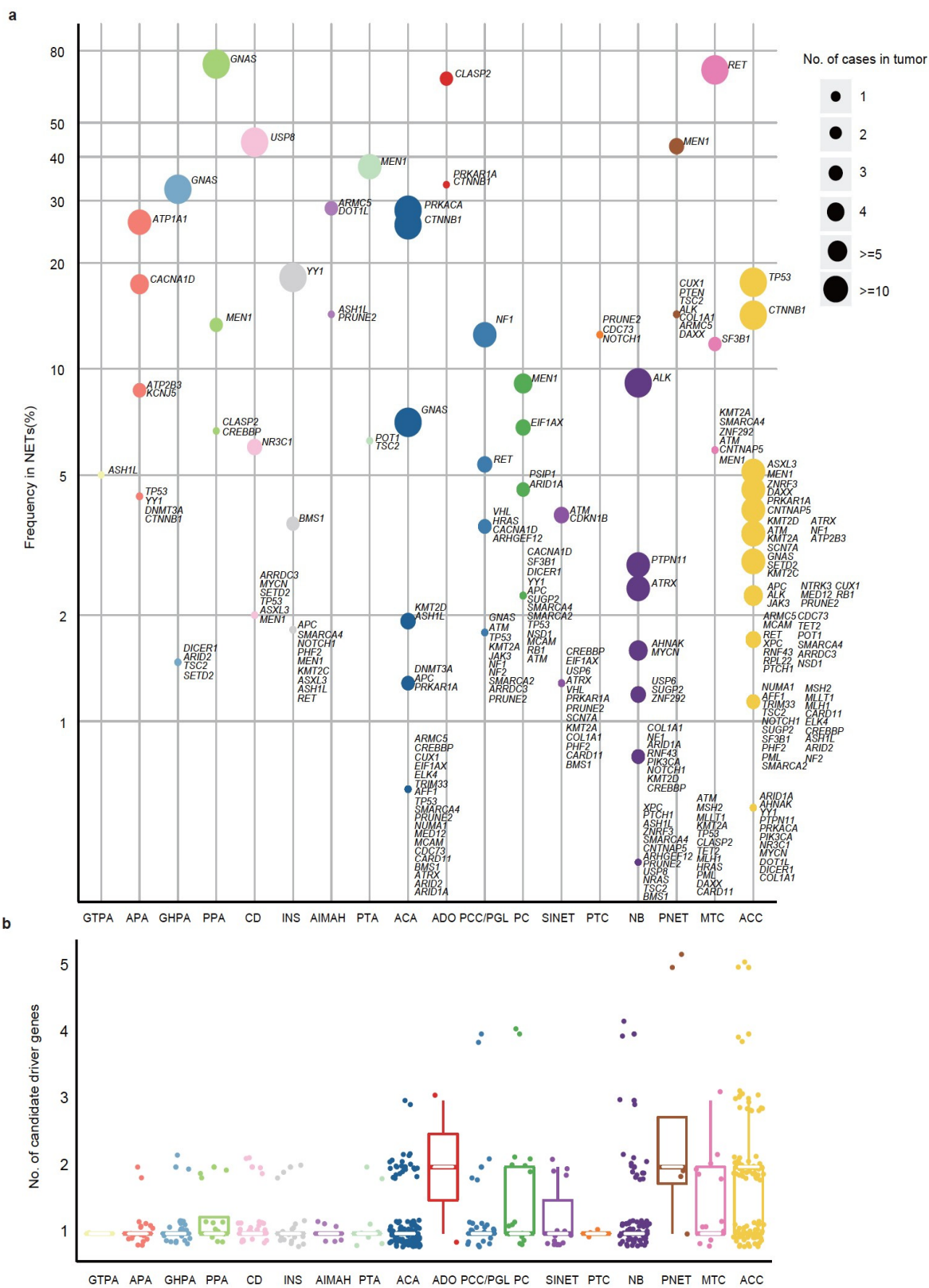
Supplementary information, Figure S8

Figure S8 The candidate driver genes identified in 21 NETs. (a) Distribution of frequencies of candidate driver genes in in each type of 21 NETs. The distribution of the 86 genes in 21 NETs revealed that malignant NETs have higher driver mutant events comparing with benign tumors. Tumor-specific driver genes, such as *PRKACA* in ACAs and *KCNJ5* in APA, have been reported[15-21,26]. **(b)** Boxplot of candidate driver genes across 21 NETs, only samples contain mutations in candidate driver genes are plotted. Mutations in 40 of these 52 genes occur frequently in other types of NETs in our integrated cohort; 34 novel SMGs are identified in NETs, including *AHNAK, ARRDC3, ASH1L, ASXL3, BMS1, CNTNAP5, ELK4, PHF2, SUGP2, ZNF292* and 24 genes in Cancer Gene Census (CGC).

Supplementary information, Figure S9

Figure S9 The mutated sample frequency of 86 candidate driver genes identified from 21 NETs. All candidate driver genes are plotted by the highest frequency in the benign (x axis) and malignant (y axis) tumor types. Genes marked with the color of the highest frequency tumor type as in Figure 1. *MEN1* and *RET* mutations, which are responsible for multiple endocrine neoplasia type 1 and type 2 syndromes respectively, are well-known drivers in multiple NET types. Mutations of 3 novel SMGs (*PRUNE2*, *ASH1L* and *ATM*) and 6 known candidate driver genes (*GNAS*, *CREBBP*, *KMT2A*, *TP53*, *SMARCA4* and *TSC2*) are identified in as least 5 NET types.
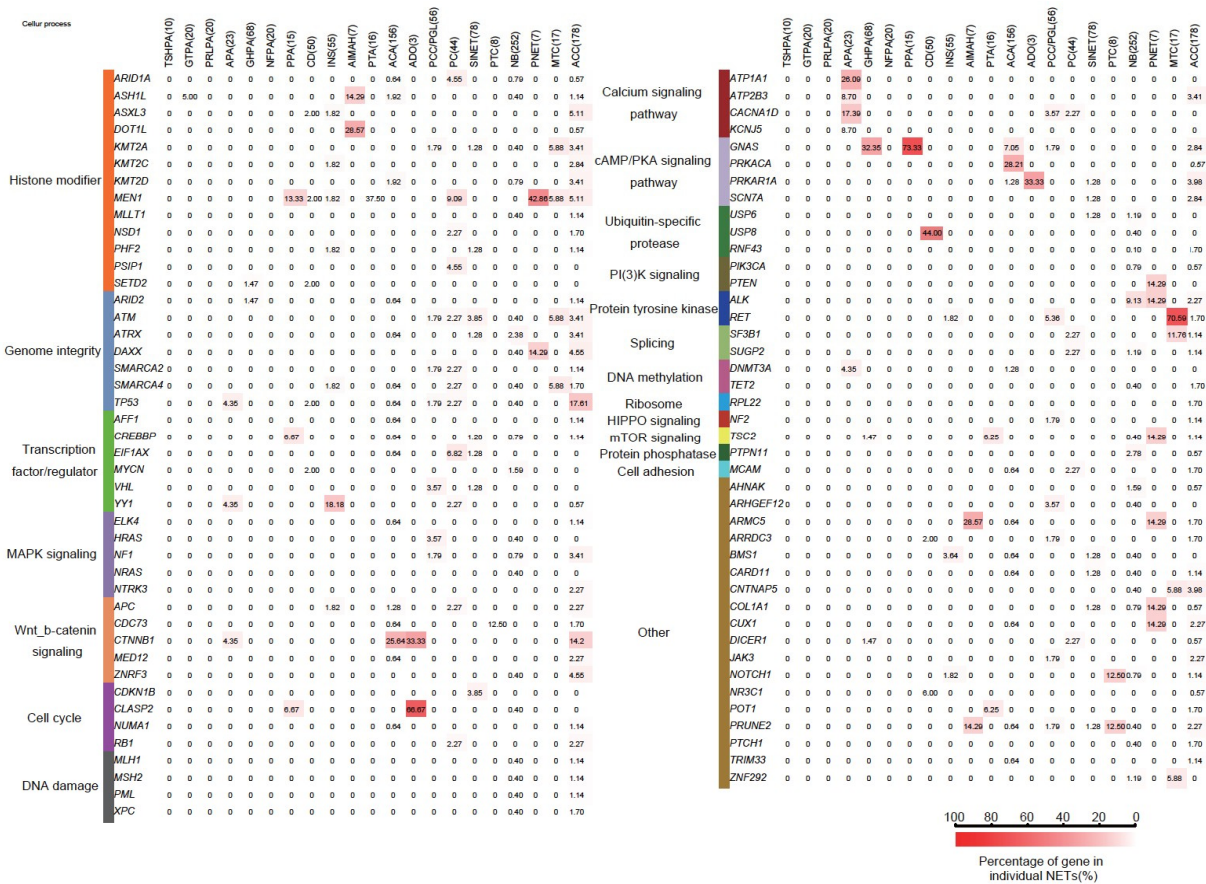
Supplementary information, Figure S10

Figure S10 The 86 candidate driver genes classified to 20 cellular processes in NETs.
Frequencies of candidate driver genes in individual tumor types are shown. The higher the
frequency of each gene in 21 NETs, the deeper the color. Mutations of *EIF1AX*, which
encodes an essential eukaryotic translation initiation factor (eIF1A) that promotes the
formation of the 43S complex, were reported in PC, papillary thyroid carcinoma and
anaplastic thyroid carcinoma[6, 58, 59]. *EIF1AX* and *SF3B1* mutations were also identified in
uveal melanomas[60]. Wnt/β-catenin signaling is activated in various NET types by mutation-
mediated blockage of β-catenin degradation. Activating *CTNNB1* and inactivating *APC*
mutations are common in adrenal NETs. In addition, mutations activating PKA signaling and
inactive *MEN1* mutations can promote Wnt/β-catenin signaling in adrenal and pancreatic
NETs[61, 62], separately. WNT negative regulators *CDC73* (*HRPT2*), *RNF43* and its homolog
ZNRF3 are SMGs in ACC[63-65]. *CDC73* is also frequently mutated in PTC[66].
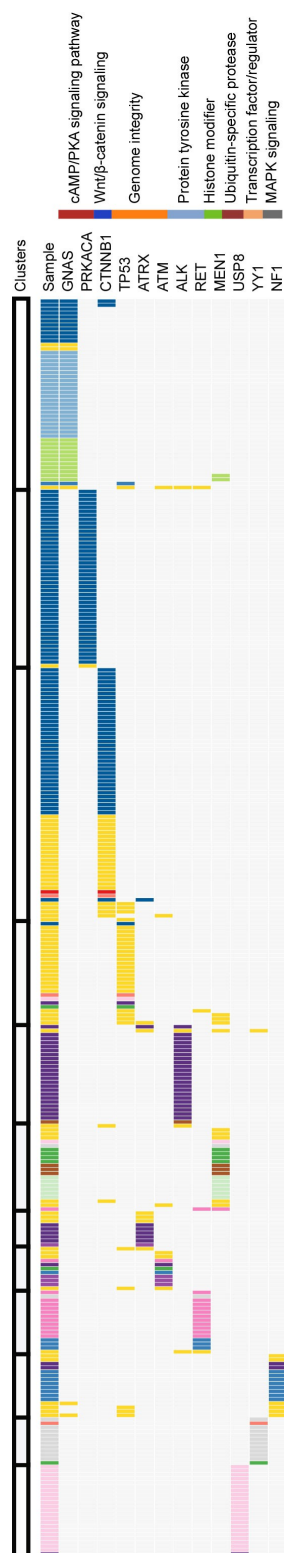
Figure S11 Clustering of cellular processes in NETs. A cellular process matrix was constructed for 317 tumors with non-silent mutations in candidate driver genes. Genes were selected with frequency more than 1% of 21 NETs. Tumors having no mutation in these genes were excluded. The tumor types are marked with the color as in Figure 1.

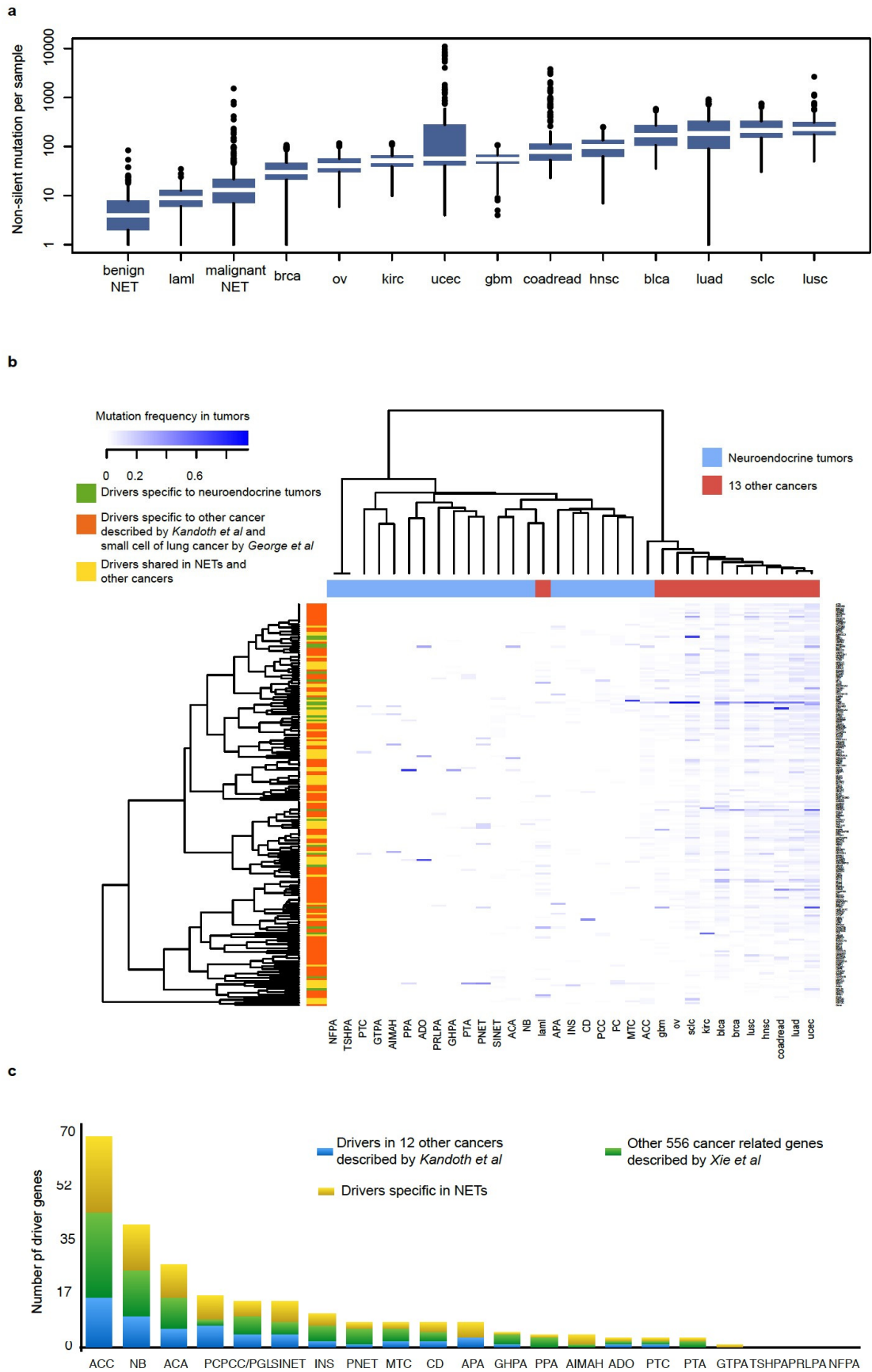# Supplementary information, Figure S12

a

b

c

Figure S12 Comparison of 86 candidate driver genes in NETs with cancer-related genes in other cancer types. (a) Non-silent mutation rate distribution of neuroendocrine tumors, 12 cancers described by Kandoth *et al.* and small cell of lung cancer (SCLC) described by George *et al*. and Rudin *et al*. The mutation frequency of benign and malignant NETs is lower compared to other cancer types. **(b)** Clustering tumors with candidate driver genes in 21 NETs and significant mutated genes in 12 cancers and SCLC. A gene frequency to each tumor type matrix was constructed. NETs shared 24 driver genes (28%) with other cancers. **(c)** Bar plot of candidate driver genes in NETs and other cancers. Malignant NETs contain more shared candidate driver gene with other types of cancer than benign NETs (*P* value = 0.013, student's *t*-test, one-sided). Comparison of the 86 genes, 127 driver genes of main cancer types and 556 cancer related genes in each NET type showed that 7 benign types of NETs are excluded with driver 127 genes[2, 67].
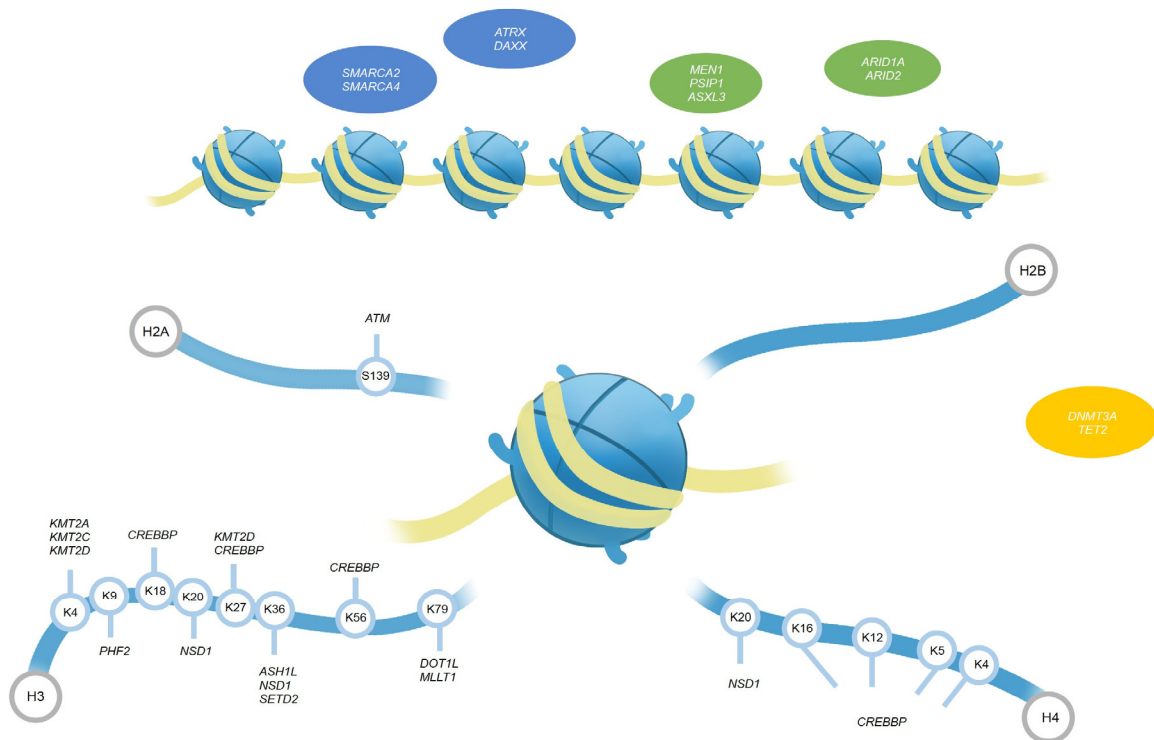
Supplementary information, Figure S13

Figure S13 Mutated genes related to chromatin remodeling and histone modification in 21 NETs. Chromatin remodeling genes: *ARID1A*, *ARID2*, *ATRX*, *SMARCA2*, *SMARCA4*; chromatin-associated adapter proteins*: MEN1, DAXX, PSIP1, ASXL3*; histone H3 methyltransferase: *ASH1L, DOT1L, NSD1, SETD2, KMT2A, KMT2C, KMT2D*; histone H3 histone demethylase: *PHF2*; histone acetyltransferases: *CREBBP*; DNA methyltransferase *DNMT3A*; active DNA demethylation: *TET2*; SWI/SNF family: *ARID1A, ATRX, SMARCA2, SMARCA4*. Ten chromatin modification and remodeling genes are identified as novel SMGs, including the SWI/SNF complex gene *ARID2*, histone H3 methyltransferase *ASH1L*, *NSD1* and *SETD2*, the DOT1L complex component *MLLT1*, histone H3 demethylase *PHF2*, DNA methyltransferase *DNMT3A* and *TET2*, histone H2A phosphorylation factor *ATM* and chromatin-associated adapter protein *ASXL3*. These SMGs were previously identified in other cancer types, suggesting shared etiologies between NETs and other cancers. *KMT2A, DNMT3A, SETD2, TET2* and *ASXL3* are significantly mutated in hematological

malignancies[68-71]. Inactivating mutations of *ARID2* are relatively common in hepatocellular carcinoma[72]. Frequent mutations of *ASH1L* were reported in esophageal squamous cell cancer and lung cancers[73, 74].
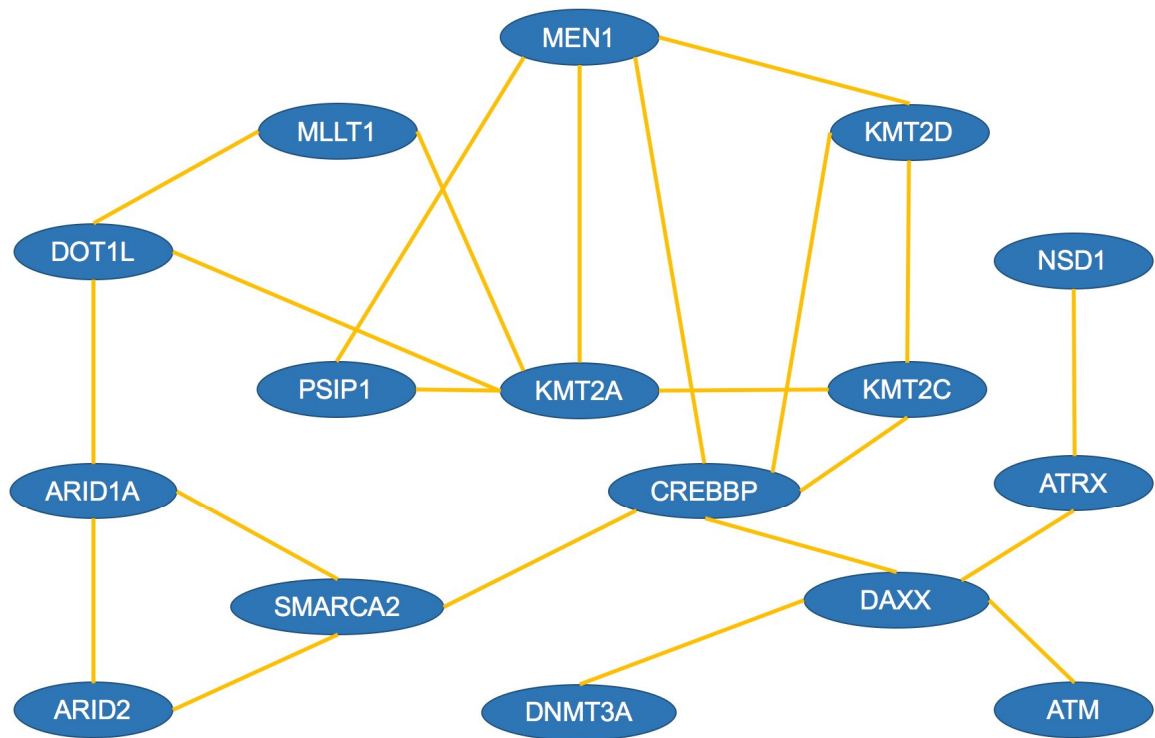
Figure S14 Protein-protein interaction network for the functional relationship of chromatin remodeling and histone modification genes in SMGs.
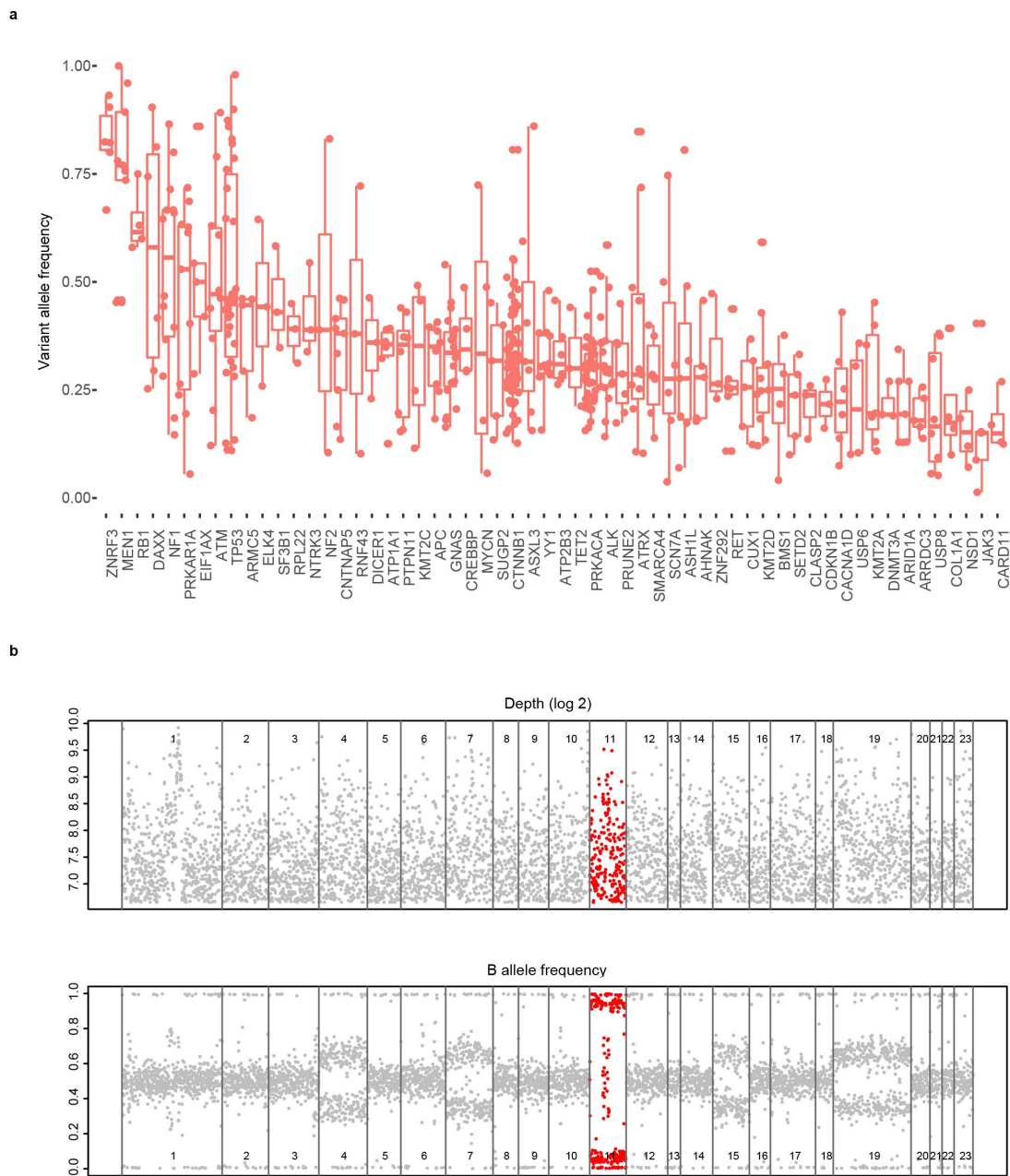
Figure S15 Variant allele frequency distribution of SMGs. **(a)** Variant allele frequency (VAF) distribution of mutations in candidate driver genes across tumors. Only mutation sites with more than 100× coverage were used for analysis and plotting. Candidate driver genes with at least 3 data points were included in the plot. The VAFs of mutations in *ZNRF2* (*P* = 1.72e-05), *MEN1* (*P* = 1.20e-04), *RB1* (*P* = 1.83e-03) are significantly higher than average among candidate driver genes. Significant levels were calculated using student's *t*-test, one-sided. The *MEN1, ZNRF3* mutations are associated with LOH as reported[18, 75]. **(b)** LOH of

MEN1 in INS. Depth and B allele frequency (higher frequency allele) of whole exonic SNP site in case INS36. The whole chromosome 11 which includes *MEN1* was identified as LOH.
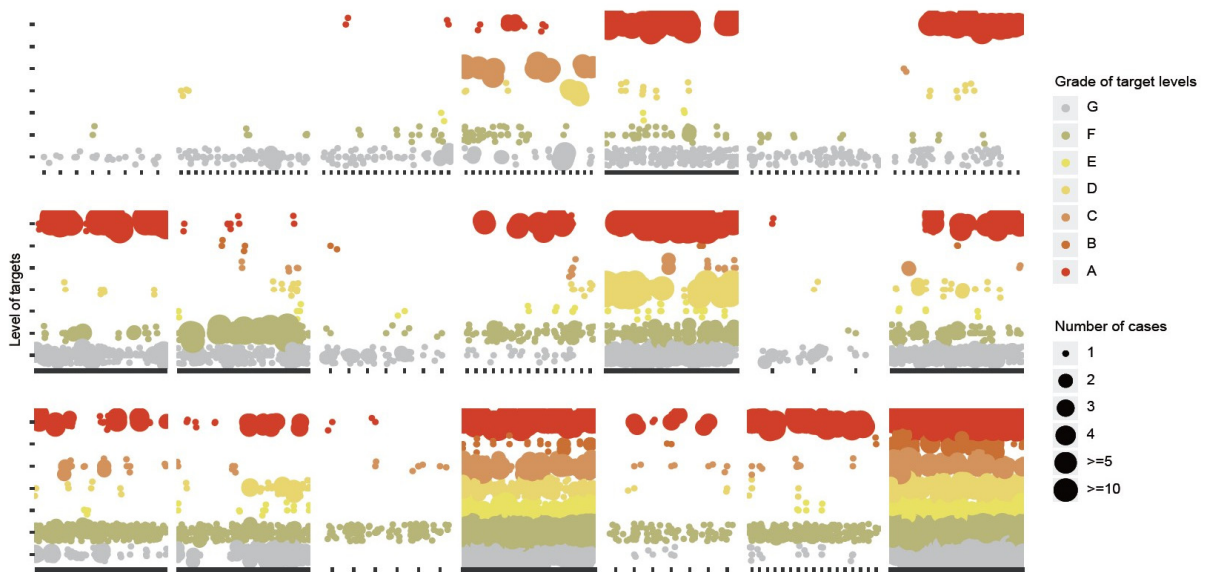
Supplementary information, Figure S16

Figure S16 Gels for 21 NETs with clinical actionable mutations. Each patient's clinical actionable somatic mutations were systematically analyzed according to druggable targets in NETs, additional biologically significant pathways and gene sets, and then ranked them by applying a series of rules on the basis of clinical and biological relevance. Level of mutations were defined as follows: A, clinically actionable mutations of NETs; B, mutations in actionable cancer genes of NETs; C, COSMIC mutations in CGC genes; D, mutations in genes that affected drugable linked pathway; E, mutations in genes that affected cancer related pathway; F, mutations in COSMIC; G, unknown mutations. Defined levels of potential targets in tumors revealed that most of the NET types (17/21) contained level A druggable mutated genes (predictive for FDA-approved therapies and in clinical trial therapies).

Supplementary information, Figure S17
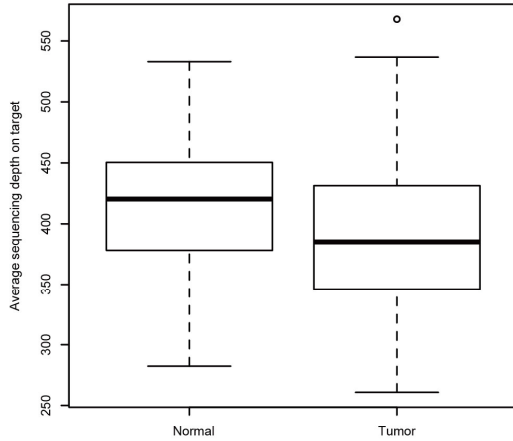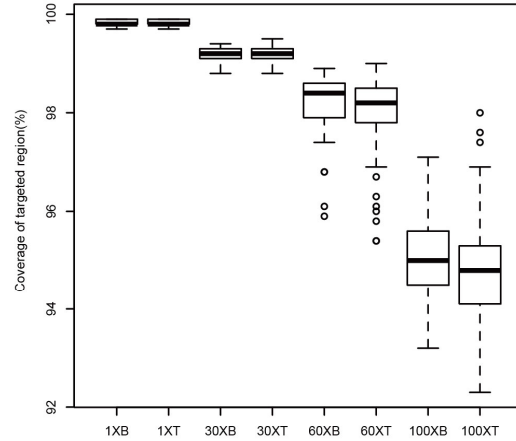
a **b**

Figure S17 Fold coverage of target regions for the pairs of APAs. (a) The box plots show the distribution of average sequencing depth of exonic regions obtained from APA samples target deep sequencing data. The bold lines in boxes represent the medians and the lines outside the boxes represent the first or third quartiles of fold coverage. **(b)** The box plots show the fraction of target bases covered by at least 1 reads, 4 reads, 10 reads and 20 reads across the target deep sequencing of APA samples. The bold lines in boxes show the medians and the lines outside the boxes show the first or third quartiles of fraction of target bases covered by reads.

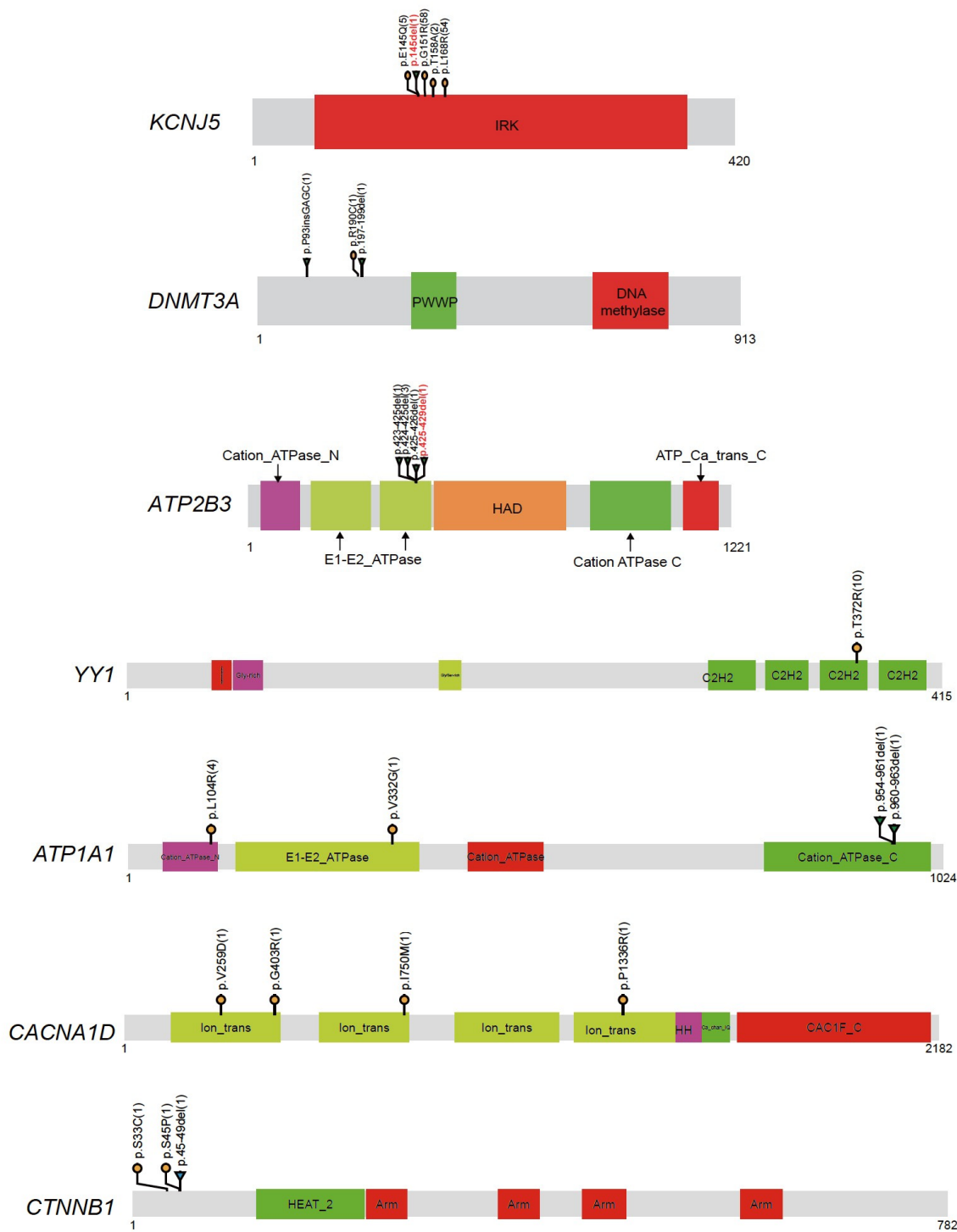# Supplementary information, Figure S18

Figure S18 Somatic mutations in *KCNJ5*, *ATP2B3*, *DNMT3A, YY1, ATP1A1*, *CACNA1D* and *CTNNB1*. Mutations annotated with red are identified as new mutations in APAs. The types and relative positions of somatic mutations are shown in the transcripts of genes using the following symbols: yellow bullets, missense mutations; green triangles, InDels. Colored regions represent domains in genes, *YY1*: red, Asp/Glu-rich (acidic); purple, Gly-rich; light green, Gly/Ser-rich; green, C2H2-type zinc fingers (ZnF_C2H2); *ATP1A1*: purple, cation transporter/ATPase, N-terminus (Cation_ATPase_N); light green, E1-E2 ATPase (E1-E2_ATPase); red, cation transport ATPase (Cation_ATPase); green, cation transporting ATPase, C-terminus (Cation_ATPase_C); *CACNA1D*: light green, ion transport protein (Ion_trans); purple, voltage-dependent L-type calcium channel, IQ-associated (GPHH); green, voltage-dependent L-type calcium channel, IQ-associated (Ca_chan_IQ); red, voltage-gated calcium channel subunit alpha, C-term (CAC1F_C); *CTNNB1*: green: HEAT repeats (HEAT_2); red: Armadillo/beta-catenin-like repeat (Arm).
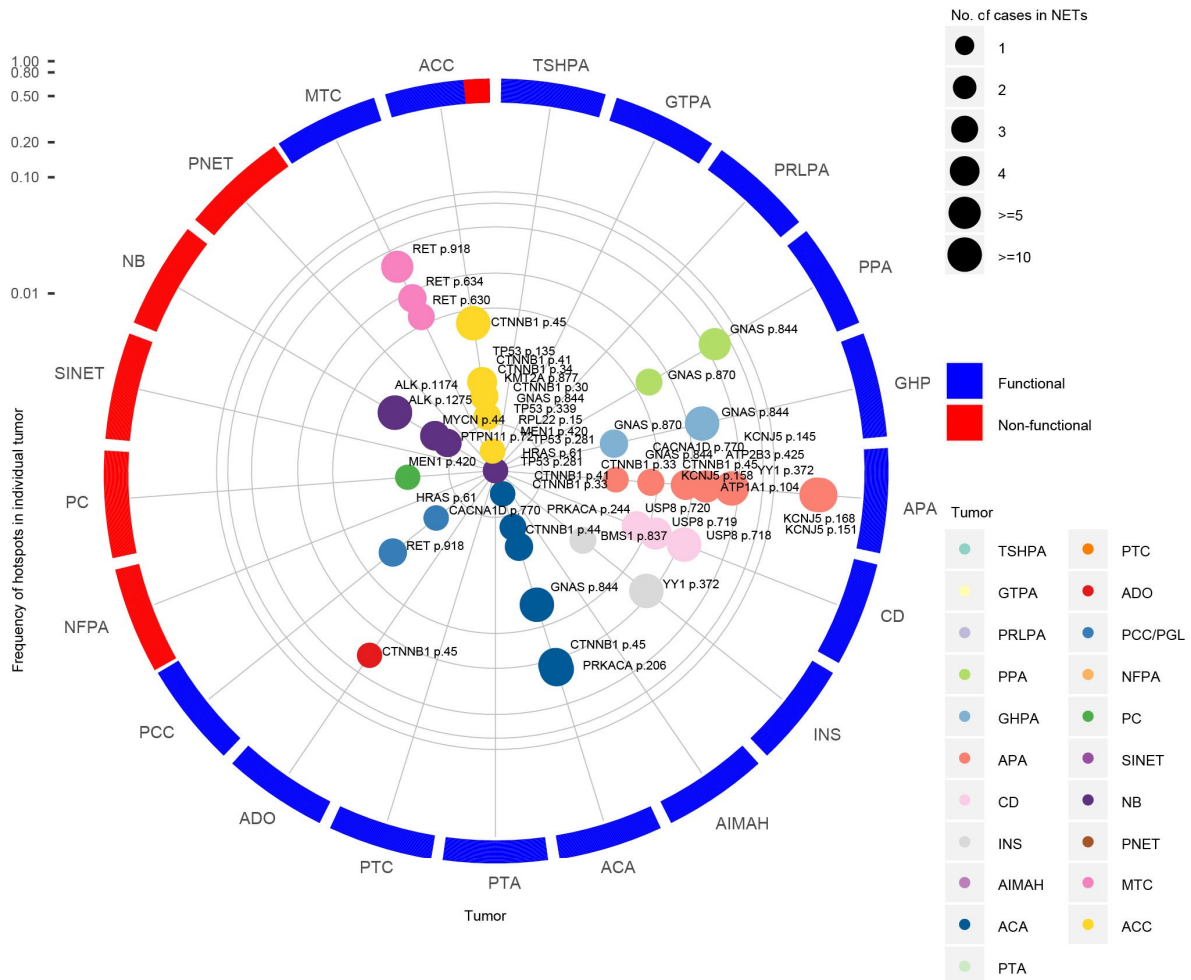
Figure S19 Hotspot mutations of candidate driver genes in 21 NETs between functional and non-functional tumors. The angular space is compartmentalized into the 21 NETs. The distance from the center represents the total mutation frequency in tumor types. The activating hotspots mutations in SMGs, including *YY1*, *GNAS*, *PRKACA*, *KCNJ5*, *USP8* and *RET*, are more frequent in functional NETs, indicating their dual roles in hormone production and tumorigenesis.

References

11. H Li, R Durbin. Fast and accurate short read alignment with Burrows-Wheeler transform. *Bioinformatics* 2009; **25**, 1754-1760.

12. Picard http://picard.sourceforge.net/ 2013.

13. McKenna A, *et al*. The Genome Analysis Toolkit: a MapReduce framework for analyzing next-generation DNA sequencing data. *Genome Res* 2010; **20**, 1297-1303.

14. Koboldt DC, *et al*. VarScan 2: somatic mutation and copy number alteration discovery in cancer by exome sequencing. *Genome Res* 2012; **22**, 568-576.

15. Cao Y, *et al.* Activating hotspot L205R mutation in PRKACA and adrenal Cushing's syndrome. *Science* 2014; **344**, 913-917.

16. Beuschlein F, *et al.* Constitutive activation of PKA catalytic subunit in adrenal Cushing's syndrome. *N Engl J Med* 2014; **370**, 1019-1028.

17. Sato Y, *et al.* Recurrent somatic mutations underlie corticotropin-independent Cushing's syndrome. *Science* 2014; **344**, 917-920.

18. Assié G, *et al.* Integrated genomic characterization of adrenocortical carcinoma. *Nat Genet* 2014; **46**, 607-612.

19. Choi M, *et al.* K+ channel mutations in adrenal aldosterone-producing adenomas and hereditary hypertension. *Science* 2011; **331**, 768-772.

20. Beuschlein F, *et al.* Somatic mutations in ATP1A1 and ATP2B3 lead to aldosterone-producing adenomas and secondary hypertension. *Nat Genet* 2013; **45**, 440-444.

21. Azizan EA, *et al.* Somatic mutations in ATP1A1 and CACNA1D underlie a common subtype of adrenal hypertension. *Nat Genet* 2013; **45**, 1055-1060.

22. Reincke M, *et al.* Mutations in the deubiquitinase gene USP8 cause Cushing's disease. *Nat Genet* 2015; **47**, 31-38.

23. Cromer MK, *et al.* Neomorphic effects of recurrent somatic mutations in Yin Yang 1 in insulin-producing adenomas. *Proc Natl Acad Sci USA* 2015; **112**, 4062-4067.

24. Välimäki N, *et al.* Whole-Genome Sequencing of Growth Hormone (GH)-Secreting Pituitary Adenomas. *J Clin Endocrinol Metab* 2015; **100**, 3918-3927.

25. Agrawal N, *et al.* Exomic sequencing of medullary thyroid cancer reveals dominant and mutually exclusive oncogenic mutations in RET and RAS. *J Clin Endocrinol Metab* 2013; **98**, E364-369.

26. Pugh TJ, *et al.* The genetic landscape of high-risk neuroblastoma. *Nat Genet* 2013; **45**, 279-284.

27. Sausen M, *et al.* Integrated genomic analyses identify ARID1A and ARID1B alterations in the childhood cancer neuroblastoma. *Nat Genet* 2013; **45**, 12-17.

28. Jiao Y, *et al.* DAXX/ATRX, MEN1, and mTOR pathway genes are frequently altered in pancreatic neuroendocrine tumors. *Science* 2011; **331**, 1199-1203.

29. Fernandez-Cuesta L, *et al.* Frequent mutations in chromatin-remodelling genes in pulmonary carcinoids. *Nat Commun* 2014; **5**, 3518.

30. Castro-Vega LJ, *et al.* Multi-omics analysis defines core genomic alterations in pheochromocytomas and paragangliomas. *Nat Commun* 2015; **6**, 6044.

31. Flynn A, *et al.* The genomic landscape of phaeochromocytoma. *J Pathol* 2015; **236**, 78-89.

32. Newey PJ, *et al.* Whole-exome sequencing studies of nonhereditary (sporadic) parathyroid adenomas. *J Clin Endocrinol Metab* 2012; **97**, E1995-2005.

33. Yu W, *et al.* Whole-exome sequencing studies of parathyroid carcinomas reveal novel PRUNE2 mutations, distinctive mutational spectra related to APOBEC-catalyzed DNA mutagenesis and mutational enrichment in kinases associated with cell migration and invasion. *J Clin Endocrinol Metab* 2015; **100**, E360-364.

34. Banck MS, *et al.* The genomic landscape of small intestine neuroendocrine tumors. *J Clin Invest* 2013; **123**, 2502-2508.

35. Francis JM, *et al.* Somatic mutation of CDKN1B in small intestine neuroendocrine tumors. *Nat Genet* 2013; **45**, 1483-1486.

36. Ronchi CL, *et al.* Genetic Landscape of Sporadic Unilateral Adrenocortical Adenomas Without PRKACA p.Leu206Arg Mutation. *J Clin Endocrinol Metab* 2016; **101**, 3526-3538.

37. Juhlin CC, *et al.* Whole-exome sequencing characterizes the landscape of somatic mutations and copy number alterations in adrenocortical carcinoma. *J Clin Endocrinol Metab* 2015; **100**, E493-502.

38. Zheng S, *et al.* Comprehensive Pan-Genomic Characterization of Adrenocortical Carcinoma. *Cancer Cell* 2016; **29**, 723-736.

39. Song ZJ, *et al.* The genome-wide mutational landscape of pituitary adenomas. *Cell Res* 2016; **26**, 1255-1259.

40. Ronchi CL, *et al.* Landscape of somatic mutations in sporadic GH-secreting pituitary adenomas. *Eur J Endocrinol* 2016; **174**, 363-372.

41. Wang K, Li M, Hakonarson H. ANNOVAR: functional annotation of genetic variants from high-throughput sequencing data. *Nucleic Acids Res* 2010; **38**, e164.

42. Yang H, Wang K. Genomic variant annotation and prioritization with ANNOVAR and wANNOVAR. *Nat Protoc* 2015; **10**, 1556-1566.

43. Chang X, Wang K. wANNOVAR: annotating genetic variants for personal genomes via the web. *J Med Genet* 2012; **49**, 433-436.

44. Cingolani P, *et al*. A program for annotating and predicting the effects of single nucleotide polymorphisms, SnpEff: SNPs in the genome of Drosophila melanogaster strain w1118; iso-2; iso-3. *Fly* 2012; **6**, 80-92.

45. Sherry ST, *et al*. dbSNP: the NCBI database of genetic variation. *Nucleic Acids Res*

2001; **29**, 308-311.

46. Dees ND, *et al*. MuSiC: identifying mutational significance in cancer genomes. *Genome Res* 2012; **22**, 1589-1598.

47. Forbes SA, *et al*. The Catalogue of Somatic Mutations in Cancer (COSMIC). *Curr Protoc Hum Genet* 2008; **Chapter 10**, Unit 10.11.

48. Ng PC, Henikoff S. SIFT: Predicting amino acid changes that affect protein function. *Nucleic Acids Res* 2003; **31**, 3812-3814.

49. Adzhubei I, Jordan DM, Sunyaev SR. Predicting functional effect of human missense mutations using PolyPhen-2. *Curr Protoc Hum Genet* 2013; **Chapter 7**: Unit 7.20.

50. Su AI, *et al*. A gene atlas of the mouse and human protein-encoding transcriptomes. *Proc Natl Acad Sci USA* 2014; **101**, 6062-6067.

51. Li T, *et al*. A scored human protein-protein interaction network to catalyze genomic interpretation. *Nat   Methods* 2017; **14**, 61-64.

52. Van Allen EM, *et al*. Whole-exome sequencing and clinical interpretation of formalin-fixed, paraffin-embedded tumor samples to guide precision cancer medicine. *Nat Med* 2014; **20**, 682-688.

53. Dienstmann R, *et al*. Standardized decision support in next generation sequencing reports of somatic   cancer variants. *Mol Oncol* 2014; **8**, 859-873.

54. Gaulton A, *et al*. ChEMBL: a large-scale bioactivity database for drug discovery. *Nucleic Acids Res* 2012; **40** (Database issue), D1100-1107.

55. Rubio-Perez C, *et al*. In silico prescription of anticancer drugs to cohorts of 28 tumor types reveals   targeting opportunities. *Cancer Cell* 2014; **27**, 382-396.

56. Van Allen EM, *et al*. Whole-exome sequencing and clinical interpretation of formalin-fixed, paraffin-embedded tumor samples to guide precision cancer medicine. *Nat Med* 2014; **20**, 682-688.

57. Subramanian A, *et al.* Gene set enrichment analysis: a knowledge-based approach for interpreting genome-wide expression profiles. *Proc Natl Acad Sci USA* 2005; **102**, 15545-15550.

58. Cancer Genome Atlas Research Network. Integrated genomic characterization of papillary thyroid carcinoma. *Cell* 2014; **159**, 676-690.

59. Kunstman JW, *et al.* Characterization of the mutational landscape of anaplastic thyroid cancer via whole-exome sequencing. *Hum Mol Genet* 2015; **24**, 2318-2329.

60. Martin M, *et al.* Exome sequencing identifies recurrent somatic mutations in EIF1AX and SF3B1 in uveal melanoma with disomy 3. *Nat Genet* 2013; **45**, 933-936.

61. Berthon A, *et al.* Wnt/β-catenin signalling in adrenal physiology and tumor development. *Mol Cell Endocrinol* 2012; **351**, 87-95.

62. Jiang X, *et al.* Targeting β-catenin signaling for therapeutic intervention in MEN1-deficient pancreatic neuroendocrine tumors. *Nat Commun* 2014; **5**, 5809.

63. James RG, *et al.* Bruton's tyrosine kinase revealed as a negative regulator of Wnt-beta-catenin signaling. *Sci Signal* 2009; **2**, ra25.

64. Hao HX, *et al.* ZNRF3 promotes Wnt receptor turnover in an R-spondin-sensitive manner. *Nature* 2012; **485**, 195-200.

65. Steinhart Z, *et al.* Genome-wide CRISPR screens reveal a Wnt-FZD5 signaling circuit as a druggable vulnerability of RNF43-mutant pancreatic tumors. *Nat Med* 2017; **23**, 60-68.

66. Shattuck TM, *et al.* Somatic and germ-line mutations of the HRPT2 gene in sporadic parathyroid carcinoma. *N Engl J Med* 2003; **349**, 1722-1729.

67. Xie M, *et al.* Age-related mutations associated with clonal hematopoietic expansion and malignancies. *Nat Med* 2014; **20**, 1472-1478.

68. Mardis ER, Recurring mutations found by sequencing an acute myeloid leukemia genome. *N Engl J Med* 2009; **361**, 1058-1066.

69. Ley TJ, *et al.* DNMT3A mutations in acute myeloid leukemia. *N Engl J Med* 2010; **363**, 2424-2433.

70. Zhu X, *et al.* Identification of functional cooperative mutations of SETD2 in human acute leukemia. *Nat Genet* 2014; **46**, 287-293.

71. Delhommeau F, *et al.* Mutation in TET2 in myeloid cancers. *N Engl J Med* 2009; **360**, 2289-2301.

72. Li M, *et al.* Inactivating mutations of the chromatin remodeling gene ARID2 in hepatocellular carcinoma. *Nat Genet* 2011; **43**, 828-829.

73. Song Y, *et al.* Identification of genomic alterations in oesophageal squamous cell cancer. *Nature* 2014; **509**, 91-95.

74. Liu J, *et al.* Genome and transcriptome sequencing of lung cancers reveal diverse mutational and splicing events. *Genome Res* 2012; **22**, 2315-2327.

75. Jiang XH, *et al.* MEN1 mutation analysis in Chinese patients with multiple endocrine neoplasia type 1. *Endocr Relat Cancer* 2007; **14**, 1073-1079.